Two-Dimensional Fine Particle Positioning Under Optical Microscope Using a Piezoresistive Cantilever as a Manipulator

Metin Sitti and Hideki Hashimoto
Institute of Industrial Science, University of Tokyo,
Roppongi, 7-22-1, Minato-ku, Tokyo, 106-8558, Japan
sitti@vss.iis.u-tokyo.ac.jp, hashimoto@iis.u-tokyo.ac.jp

Abstract

In this paper, a fine particle manipulation system using a piezoresistive microcantilever, which is normally utilized in Atomic Force Microscopy, as the manipulator and force sensor, and a top-view Optical Microscope (OM) as the vision sensor is proposed. Modeling and control of the interaction forces among the manipulator, particle and surface have been realized for moving particles with sizes less than 3 μm on a silicon substrate in 2-D. The microcantilever behaves also as a force sensor which enables contact point detection, real-time force measurements, and surface alignment sensing. A 2-D OM real-time image feedback constitutes the main user interface, where the operator uses mouse cursor and keyboard for defining the tasks for the cantilever motion controller. Preliminary particle manipulation experiments are demonstrated for 2.02 and 1 μm gold-coated latex particles, and it is shown that the system can be utilized in 2-D micro particle assembling.

Keywords: Micro/nanorobotics; Atomic Force Microscopy; micro/nanophysics; micro/nano-assembly; task-based control.

1 Introduction

By the recent advances on micro-mechatronics technology, micro sensors and actuators, high precision positioners, microrobots inside the nuclear plant pipes, and etc. have become possible. Especially, imaging devices such as Scanning Probe Microscopes and Near-Field Optical Microscope can provide imaging down to sub-micron and atomic scale at 2-D or 3-D. However, for constructing more complex micro/nano machines or devices by assembling micro/nano parts, necessary fabrication and manipulation technologies are still very immature at the scales less than 10 μm. Because, at these scales, micro/nano sticking forces become dominant to the inertial force, and a new robotic approach is indispensable. By such a new micro/nanorobotics field, precise and local manipulation of objects at the micro/nano scale is aimed. Such field can enable future micro/nanotechnological applications such as constructing micro/nano devices and machines, terabyte hard-disk memories, DNA-computers, and etc. that would have revolutionary impacts.

One of the most challenging problems of the micro/nanorobotics is the micro/nano-assembly. For assembling micro/nano objects such as particles, different tools or control approaches have been proposed. Miyazaki *et al.* [1] proposed a two probe-based directly teleoperated assembly of spherical latex particles with the diameter of approximately 2 μm in 3-D, and tried to construct a 3-D pyramid where they had problems of assembling the last top particle due to adhesive forces. Tanikawa *et al.* [2] developed a directly teleoperated two-finger micro hand like a chopstick for moving glass spheres in 3-D with the size of 2 μm. Pappas *et al.* [3] proposed a robotic system where a micro/nano-tool is driven automatically for realizing simple tasks using visual servoing. They achieved positioning of 50 μm diameter diamond particles using a glass pipette with air pressure controlled picking and placing. Recently, significant attention is also being paid for the contact and adhesive force understanding for introducing reliable micromanipulation strategies [4], [5], [6], [7], [8], [9], [10].

In this paper, a task-based semi-autonomous 2-D fine particle assembly system which utilizes Optical Microscope (OM) as the vision sensor, and piezoresistive Atomic Force Microscope (AFM) cantilever with its tip as the micro/nano manipulator and force sensor is proposed. As different from other works, the proposed system has the potential of also manipulating the nano objects by replacing the OM imaging with the AFM non-contact imaging [11], [12], [13], [14], the manipulator and force sensor are integrated which enables a compact and cost-effective manipulator that would be also used as a gripper of future micro scale robots, real-time force feedback enables the measurement of the interaction forces during the manipulation and understanding of the underlying physical phenomenon by introduced analytical models, and even using one optical microscope, the depth (distance between the substrate/particle and AFM probe tip) information is obtained through the tip-substrate contact feedback.

The organization of the paper is as follows: at first, the fine particle assembly problem and our approach are defined. Then, the system setup and its components such as AFM, vision sensor, position control, and etc. are explained. Next, the analysis of manipulation forces is given, and micro particle assembly experiments are described. Finally, conclusions and future directions are reported.

2 Problem Definition and Approach

Spherical polyvinyl gold-coated latex particles with sizes around 2.02 and 1 μm (JEOL Datum Ltd., Japan) are semi-fixed/absorbed to a silicon substrate such that they are to be positioned by changing their x-y positions [15], [16]. The particles are also called as *absorbates*. By reducing the limitations on the environment for easy and cost-effective mechanical design, the operations are to be realized in ambient conditions with the relative humidity of $40-50\%$, and the temperature of $23-25\ C^o$. Thus, the sticking forces such as capillary and van der Waals forces exist, and the former would be dominant with respect to the latter. Here, it is assumed that the electrostatic forces are negligible with respect to other sticking forces.

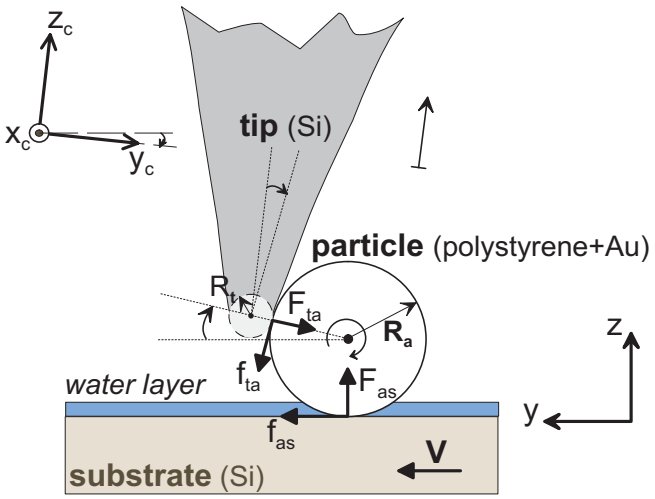

Figure 1: Positioning of the fine particles using the AFM tip as the contact pushing/pulling manipulator.

The cantilever tip which has a radius $R_t = 25-30\ nm$ is being utilized in contact pushing or pulling of the particles. Assuming the tip is pushing from a contact point passing through the absorbate center, the 3-D system can be simplified to 2-D as shown in Figure 1. The extension of the formulation to the 3-D case without assumption is direct. In the figure, F_{ta} and f_{ta} correspond to the tip-absorbate attractive/repulsive interaction force and friction force, and F_{as} and f_{as} are the the absorbate-substrate interaction and friction forces respectively. The angle between the contact point of the tip and particle center is represented as β ($\in [0, \pi/2)$ for pushing). The tip is aligned with an angle $\alpha \in [0, \pi/4]$. The tip is placed above the substrate with the parking height equals to the radius of the particle R_a. Thus, it is assumed not to touch to and interact with the substrate. By this way, the tip is not deformed, and adhesion forces between the tip and particle is reduced by a point-contact.

Here, not the tip base but the substrate is moved with a constant speed V, and the manipulation strategy is as follows: *use the fixed cantilever as a stopper while moving the substrate under the particle with a uniform speed.*

The aim is to design the control parameters such as the contact point and angle, cantilever properties such as stiffness and tip radius and shape, particle-substrate friction, adhesion forces,

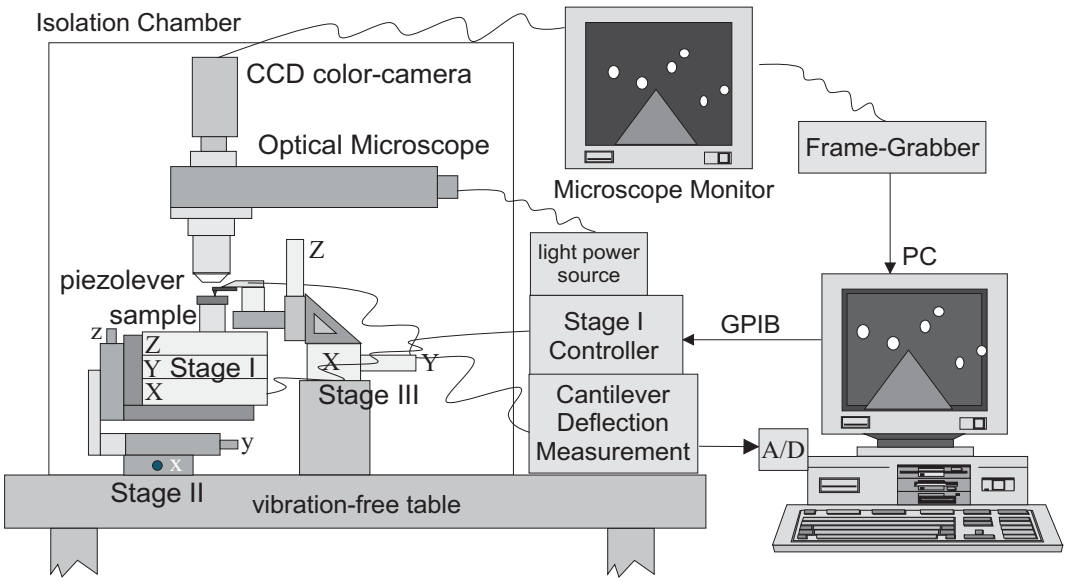

Figure 2: Overall system setup for the fine particle assembly.

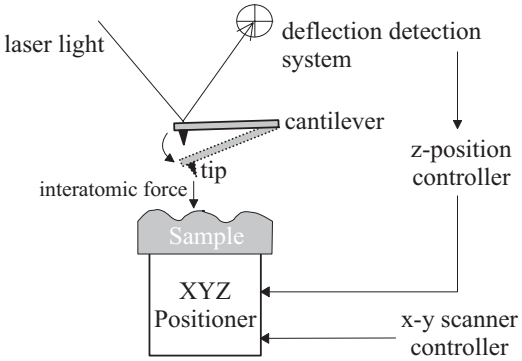

Figure 3: The basic structure of a conventional AFM.

humidity level and motion resolution and speed so that particles can be positioned in 2-D precisely.

3 System Setup

A task-based teleoperation control approach is selected [4] where an operator determines the tasks to be realized, and a controller realizes these tasks automatically. The overall system is shown in Figure 2.

3.1 *AFM as the Manipulator and Sensor*

The basic structure of a conventional AFM system is shown in Figure 3. The very sharp cantilever tip atoms are interacted with the sample atoms by moving the sample (or cantilever) in the z-

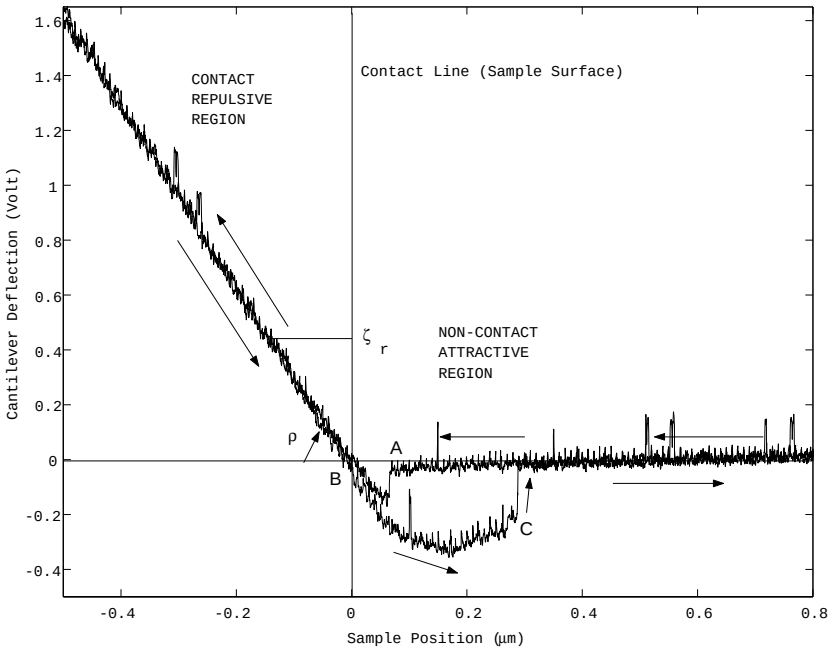

Figure 4: The typical cantilever deflection, i.e. inter-atomic force, and sample position relation for a silicon sample (experimental).

direction. The z-direction inter-atomic force $F_n(t)$ is attractive or repulsive, and the resulting typical deflection curve of the cantilever $\zeta(t)$ depending on the sample position $z(t)$ is shown in Figure 4. In the figure, the sample is moved towards the tip where after the point A, the long-range attractive forces such as van der Waals or electrostatic forces bend the cantilever to a negative value with a nonlinear function. Following a maximum peak, this attractive force comes to zero at the contact point B where $z = a_0$ with $a_0 \approx 0.2\ nm$. If the sample is moved more, the inter-atomic repulsive forces bend the cantilever almost linearly in the contact region. After retracting the sample back, the elastic or plastic deformation is restored, and there is a bigger attractive peak due to the adhesion and other mechanical factors [14]. This attractive peak ends with the separation of the tip and sample surfaces at the point C. Then, the interactive forces become almost zero.

If the sample is moved slowly, i.e. the cantilever is assumed to be at equilibrium at each point, then

$$F_n(t) = k_c \zeta(t), \tag{1}$$

where k_c is the previously known cantilever spring constant. Thus, the tip-sample force can be measured by measuring $\zeta(t)$. Instead of an optical deflection detection system, $\zeta(t)$ is measured by a Wheatstone bridge-based deflection measurement electronics in our system as shown in Figure 5 where a piezoresistive cantilever (Park Scientific Instruments Co., USA) [17] is used. Thus, the output of the bridge is a voltage difference $V_{out}(t)$, and the nanometer value of the $\zeta(t)$ is computed from the below equation:

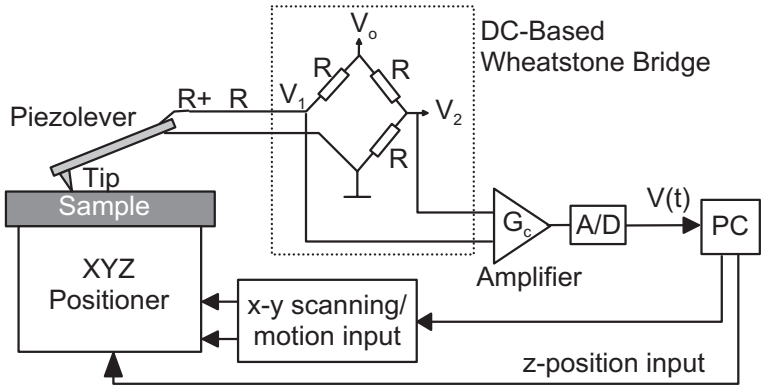

Figure 5: AFM with piezoresistive cantilever and electronic deflection detection system.

$$\zeta(t) = SG_2(G_1 V_{out}(t) + V_{off}), \tag{2}$$

where $G_1 = G_2 = 100$ are the amplification gains, V_{off} is the offset voltage which changes for each cantilever due to the variable resistance values depending on the fabrication, $V_0 = 2.5\ V$ is the bridge voltage, $R = 2\ K\Omega$, and S is the constant scaling ratio which is calibrated for each cantilever previously.

Using the Eq. (1) and $\zeta(t)$ vs. $z(t)$ relation curve, if a reference ζ_r is set at the contact linear region, then the z-stage is moved until detecting this point as shown in Figure 4, and the (x, y) positions are scanned and at each point the same reference is tracked. Thus, the surface 3-D topology image can be held. This method is called *Contact Imaging Mode*.

Above features of the AFM can be utilized during manipulation in following ways:

- interaction force feedback can be provided in real-time,
- the alignment error of the substrate can be compensated by getting a contact 3-D topology planar image of the substrate along single x and y lines where there is no particle,
- the contact point between the tip and the particle can be detected by measuring $\zeta(t)$.
- the depth information can be obtained through the cantilever substrate contact feedback.

working distance	25 mm
image resolution	$\approx 95\ nm/pixel$
lens magnification	$\times 80$
lens numerical aperture	0.5
overall magnification	$\times 5000$ (on monitor)
focusing	manual
base stand	5 d.o.f. (manual)

Table 1. Top-view Optical Microscope specifications.

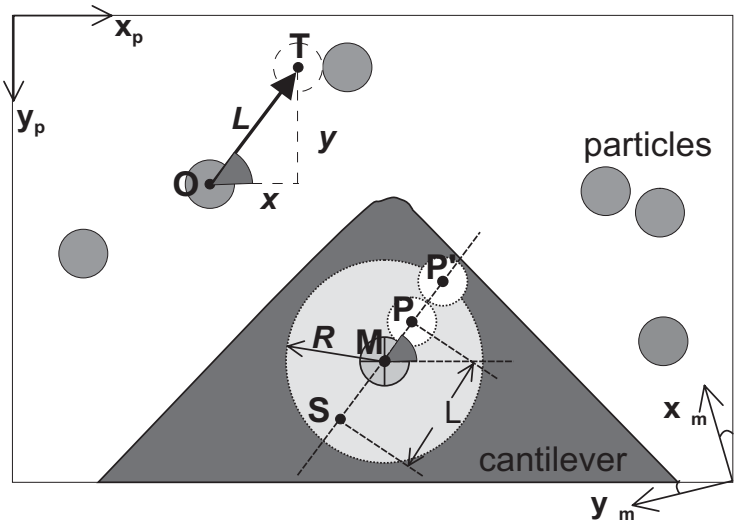

Figure 6: Automatic pushing or pulling operation, and image and positioner coordinates.

3.2 *Vision Sensor: Optical Microscope*

A reflecting light-type Optical Microscope (OM) (Olympus Co., Japan) is used as the top-view vision sensor. The specifications of the microscope is given in Table 1. A color camera (Sony Co., Japan) on the OM is connected to a Meteor frame-grabber (Matrox Co., USA) which enables real-time color image viewing of the micro world on the PC screen with the range of 640×480 $pixel^2$ in the image frame, (x_p, y_p), and approximately 59×45 μm^2 in the world coordinates, $(x_{\mu m}, y_{\mu m})$. Hereafter, the world coordinates mean the coordinate frame for the AFM positioner x-y motion space. The image and world coordinate frames are given in Figure 6. In the case of linear mapping between both spaces, $x_{\mu m} = \alpha_x x_p$ and $y_{\mu m} = \alpha_y y_p$ where $\alpha_x = \alpha_y \approx 0.095$ $\mu m/pixel$ are the x and y scaling factors. However, during the experiments, it is observed that there is also some rotation in the coordinates due to the orientations of the camera, stage and sample surface. Therefore, a calibration process is needed before the experiments in order to map (x_p, y_p) to $(x_{\mu m}, y_{\mu m})$ which is explained later.

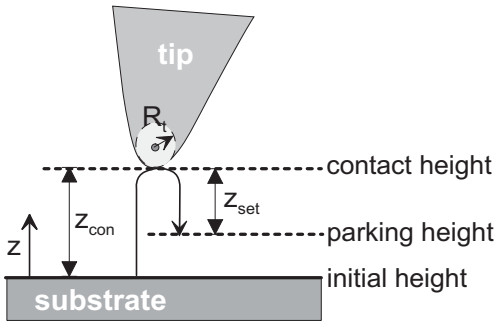

Figure 7: Parking height setting for the tip.

3.3 *User Interface*

The user interface consists of the real-time display of the top-view images from the camera mounted on the OM. The operator uses the mouse cursor and keyboard for defining the tasks for the AFM position controller. At present there are three main tasks:

- *Task 1 (T1)*: position the tip above the substrate,
- *Task 2 (T2)*: point-to-point relative motion,
- *Task 3 (T3)*: automatic pushing or pulling.

At the task *T1*, the tip is set to the height of z_{set} above from the substrate automatically. For this, the substrate is moved along the z-direction until touching to the tip, i.e. tip deflection is measured as ζ_{set}, then retracted back to the z-position given as $z = z_{con} - z_{set}$ where z_{con} is the contact height as shown in Figure 7.

In the task *T2*, using the mouse cursor, the operator clicks a point and its target point to be moved. Then the position controller automatically moves with the amount of relative distance between the two points. This operation is needed for searching and initially positioning the particles on the screen.

The task *T3* is used for semi-autonomous particle pushing or pulling. Freezing the continuous image, the operator selects the particle to be moved by clicking on the particle. Using image processing, the particle center $\mathbf{O}$ is automatically located. Next, the target position $\mathbf{T}$ is clicked by the operator. Then the pushing or pulling operation is realized automatically by moving the particles (instead of the probe tip) as shown in Figure 6 by the following strategy:

- *Step 1:* the tip radius R_t and center position $\mathbf{M}$, particle center position $\mathbf{O}$ and radius R_a, and the target position $\mathbf{T}$ are computed or known,
- *Step 2:* compute the relative distance and orientation between $\mathbf{O}$ and $\mathbf{T}$ such that

$$\begin{aligned} \Delta x &= x_T - x_O, \\ \Delta y &= y_T - y_O, \\ \theta &= tan^{-1}(|\Delta y|/|\Delta x|), \\ s_x &= \Delta x/|\Delta x|, \\ s_y &= \Delta y/|\Delta y|, \end{aligned} \tag{3}$$

- *Step 3:* find the point $\mathbf{P'}$ which is the initial set point before tip-particle contact such that

$$\begin{aligned} x_{P'} &= x_M + s_x R cos\theta, \\ y_{P'} &= y_M + s_y R sin\theta, \\ R &= R_t + 3R_a, \end{aligned} \tag{4}$$

- *Step 4:* move the substrate $3R_a$ downward from the tip for avoiding any possible collision between the tip and particle,
- *Step 5:* move from **O** to **P'** using *T2*,
- *Step 6:* move back the tip to its parking height using *T1*,
- *Step 7:* find the contact point **P** by moving from **P'** through **M** by measuring the cantilever deflection,
- *Step 8:* compute the point **S** where

$$\begin{aligned} x_S &= x_P - s_x \Delta L cos\theta, \\ y_S &= y_P - s_y \Delta L sin\theta, \\ \Delta L &= (\Delta x^2 + \Delta y^2)^{1/2}, \end{aligned} \tag{5}$$

- *Step 9:* move from **P** to **S**,
- *Step 10:* move from **S** to **O**.

3.3.1 *Selection of the Particle*

The operator clicks any (x, y) point on the particle. Assuming that the approximate maximum pixel area of the particle $\lambda_x \times \lambda_y$ is known (it is learned by preliminary tests), a window is created with left-up corner $(x-\lambda_x, y-\lambda_y)$ and right-bottom corner $(x+\lambda_x, y+\lambda_y)$. Inside of this window each pixel (i, j) with the color light intensity I_{ij} is checked such that:

initially, $m_x = m_y = n = 0$,
for all (i, j) *pixel points inside of the window:*
if $I_{ij}^{red} > T_p$ *and* $I_{ij}^{blue} > T_p$ *and* $I_{ij}^{green} > T_p$,
$m_x = (m_x + i)/(n + 1)$,
$m_y = (m_y + j)/(n + 1)$,
$n = n + 1$.

where m_x and m_y are particle center x and y positions, n is the number of detected particle pixels, and T_p is the color intensity threshold which is determined by the operator previously. Thus, $x_O = m_x$ and $y_O = m_y$ are computed.

3.4 *Tip Position Calibration*

Since the OM images are top-view images, the AFM cantilever tip which is at the bottom part of the cantilever cannot be seen directly by the microscope (it is approximately 7 μm inside from the end of the cantilever). Also, since the position of the tip can differ for each cantilever, a calibration procedure for each cantilever is necessary before the experiments. For this purpose, initially a particle is aligned closely to the end of the cantilever end as can be seen in Figure 8. The particle center position in the image coordinates, (x_O, y_O), is calculated

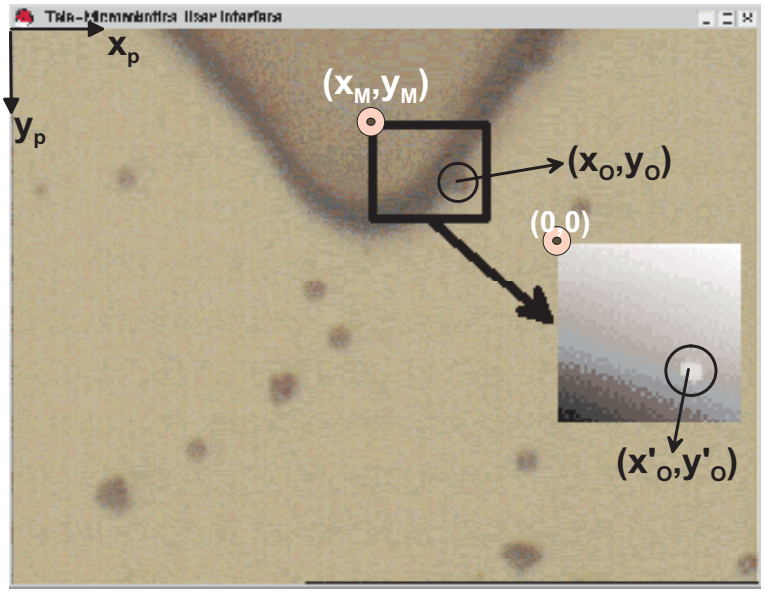

Figure 8: Automatic tip center position calibration using the tapping mode AFM imaging and selecting a 1 μm size particle close to the end of the cantilever end with a known center position in the image coordinates.

by clicking on it where the automatic particle center detection algorithm computes the exact center position. Then, by a tapping mode scanning of the sample [14] by an enough range (approximately 15×15 μm^2), the particle center is found inside of the AFM gray-scale topology image automatically by thresholding the height data, and averaging those thresholded data. Thus, the tip center position (x_M, y_M) as the top left corner point of the AFM image display is computed as: $x_M \approx x_O - x_O^{'}\Delta/\alpha_x$ and $y_M \approx y_O - y_O^{'}\Delta/\alpha_y$ where $(x_O^{'}, y_O^{'})$ are the particle center pixel position in the AFM image coordinate frame, and Δ is the xy scanning motion step size.

3.5 *Cantilever Sensitivity Calibration*

S constant which scales the voltage deflection data to nm is computed as the slope of linear deflection line in the contact region (in Figure 4, $S = tan\rho$) for a very hard surface such as mica. For the cantilevers used in the experiments, $S = 34$ nm/V with $\pm 10\%$ difference range.

3.6 *Position Control*

For the manipulation of the particles and initial settings, three different XYZ stages are utilized. Their specifications are given in Table 2. Stage I, the fine positioning XYZ piezoelectric stage (Physick Instrumente Co., Germany) with integrated LVDT (Linear Variable Differential Transformer) sensors at each axis, and closed-loop PI control is utilized during the automatic particle assembly control. The other two manual stages are used for initial alignment, cantilever focusing and particle search on the surface. The main motion of the Stage I is point-to-point motion with constant sampling time of T_s. The x and y axes should be moved simultaneously for

Stage No	*I*	*II*	*III*
Actuator	piezoelectric	bearing	bearing
Resolution	10 nm	12.5 μm	10 μm
Range	100 μm	15 mm	18 mm
Control	automatic	manual	manual
Hystheresis	$< 0.1\%$		

Table 2. Specifications of the used XYZ stages.

a linear 2-D motion where it is achieved with fast DAC board inputs to the position controller through the PC software control in our system. T_s is limited by the dynamics of the Stage I where $T_s = 30\ msec$ for the x-y axes, and $T_s = 25\ msec$ for the z-axis during the experiments.

For the point-to-point motion with constant speed $V = \Delta/T_s$, i.e. moving from (x_1, y_1) to (x_2, y_2) point, following stair-wise point-to-point motion strategy is introduced:

$$\begin{aligned} x_i &= x_1 + i(s_x \Delta cos\delta) \\ y_i &= y_1 + i(s_y \Delta sin\delta) \end{aligned} \tag{6}$$

where $i = 1, \ldots, N$, $N = \Delta L/\Delta$, Δ is the predetermined motion step resolution, s_x, s_y, θ and ΔL are computed as the equations (3) and (5) for the case of $\Delta x = x_2 - x_1$ and $\Delta y = y_2 - y_1$. Thus, at each i^{th} step, x_i and y_i are moved simultaneously.

3.7 *Coordinate Frame Calibration*

Image to world coordinates transformation constitutes of scaling, rotation and translation transformations. Rotation transformation is due to the misalignment of the substrate surface and OM image plane, and pan and tilt errors due to the rough manual positioner. For this purpose, a selected particle is tracked automatically during a controlled x-y motion. Particle detection image processing part is the same with the selection of the particle procedure. As an example, a selected 1 μm size latex particle center pixel positions are tracked during a scanning motion with 1 μm steps automatically. Using the necessary transformations, these pixel center positions are transformed to the stage x-y motion coordinates as given in Figure 9. This transformation can be expressed by the following equation:

$$\begin{bmatrix} x_{\mu m} - X_0 \\ y_{\mu m} - Y_0 \end{bmatrix} = \begin{bmatrix} cos\phi & -sin\gamma \\ sin\phi & cos\gamma \end{bmatrix} \begin{bmatrix} \alpha_y(480 - y_0 - y_p) \\ \alpha_x(640 - x_0 - x_p) \end{bmatrix}, \tag{7}$$

where $(x_{\mu m}, y_{\mu m})$ is the computed x-y stage position, (x_p, y_p) is the image coordinate pixel position (Figure 6), (X_0, Y_0) is the stage initial position before the scanning, (x_0, y_0) is the selected particle initial pixel center position, and ϕ and γ are the rotation angles. The transformation parameters are calibrated before the experiments from the graph in Figure 9. For the given figure, computed

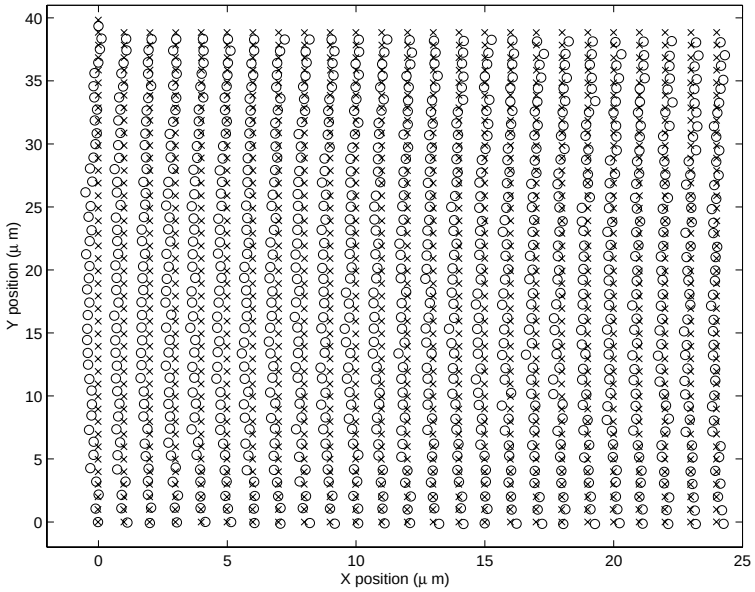

Figure 9: Controlled x-y scanning of the Stage I, and automatic tracking of the selected particle ('x' stands for the stage x-y position, and 'o' does for the transformed particle center position) for the calibration of the image to stage coordinate frame transformation.

parameters are $\alpha_x = 0.096$, $\alpha_y = 0.095$, $\phi = -2.5^o$ and $\gamma = -3^o$. As the calibration error criterion, average error distance is defined as:

$$\epsilon = \sum_{i=1}^{M} \{(X^i_{\mu m} - x^i_{\mu m})^2 + (Y^i_{\mu m} - y^i_{\mu m})^2\}^{1/2}/M \ , \tag{8}$$

where $(X^i_{\mu m}, Y^i_{\mu m})$ is the stage i^{th} xy actual position, and M is the number of the computed center positions such that for the given graph $\epsilon = 0.330\ \mu m$. ϵ should be minimized for precise manipulation while the minimum value is limited by the mechanical noise and deformation due to the horizontal table (or OM) vibration, fixed focusing blurring if the substrate is not aligned flatly, and nonhomogenous particle light reflection depending on its material type and 3-D shape.

3.8 *Substrate Alignment Calibration*

Computing the ϕ and γ alignment angles of the substrate surface by the OM calibration, it is possible to correct the x-y motion. However, also the z-position should be aligned correctly during the pushing operation where z_{set} parking height can change due to the height changes along the surface. For solving this problem, Contact-Mode AFM imaging is utilized for computing the surface alignment along the x-y axes. Selected two lines along the stage x and y axis which do not pass through particles are scanned, and the topology is measured. From these two line slopes, x and y alignment angles are computed for precise z-positioning.

4 Analysis of Interaction Forces

For reliable control of the particle x-y position, forces during approaching and pushing are analyzed. In this analysis, it is assumed that the contacting point of the cantilever tip behaves as a sphere of radius R_t during the force interaction while the whole tip shape is taken as a cone, electrostatic forces are negligible, and objects can be deformed. Furthermore, as the notation, '$-$' forces mean attractive, and '$+$' ones do the repulsive forces.

4.1 *Initial Tip-Particle Approach*

In this case, the tip is approaching to the particle, i.e. not in contact yet. Then, $f_{ta} = 0$, and F_{ta}, F_{as} and f_{as} can be modeled using the capillary and van der Waals forces, and equilibrium equations and force models are as follows:

$$\begin{aligned} F_{as} &= 4\pi\gamma R_a \ , \\ F_{ta}(h(t))) &= \frac{H\widetilde{R}}{6h(t)^2} + \frac{2\pi\gamma\widetilde{R}cos\delta}{1+\frac{(h(t)-a_0)}{2r_1}} \ , \\ f_{as} &= F_{ta}cos\beta \ , \\ F_L &= F_{as} - F_{ta}sin\beta \ , \end{aligned} \tag{9}$$

where γ is the water surface energy, F_L is the compressive load, $h(t) \geq a_0$ is the tip-particle distance during the approach, r_1 is the meniscus curvature radius, H is the Hamaker constant (for the case of a liquid layer on the sample, $H = \{(H_{tip} - H_{liquid})(H_{sample} - H_{liquid})\}^{1/2}$ [18]), $\widetilde{R} = R_a R_t/(R_a + R_t)$, $a_0 = 30^{-1/6}\sigma$ is the contact point where σ is the inter-atomic distance, $K = 4/(3\pi)((1-\nu_t^2)/E_t + (1-\nu_p^2)/E_p)^{-1}$ is the equivalent Young modulus where E_t and E_p are the Young modulus and ν_t and ν_p are the Poisson's coefficients of the tip and particle respectively, and δ is the liquid contact angle. In the case of micro scale particle size, $R_a/R_t >> 1$, and $\widetilde{R} \approx R_t$. Furthermore, F_{ta} becomes maximum at $h = a_0$ such that $F_{ta}(max) \approx 2\pi\gamma R_t$. For not moving the particle during the approach, the following condition should be provided:

$$f_{as} < \mu F_L \ , \tag{10}$$

where μ is the maximum static friction coefficient between the particle and substrate. Using the equilibrium equations and $F_{ta}(max)$,

$$\mu > \frac{R_t cos\beta}{2R_a - R_t sin\beta} \ . \tag{11}$$

For example, if $R_a = 1\ \mu m$, $R_t = 30\ nm$, and $\beta = \pi/10$, $\mu > 0.015$ for not moving the particle.

4.2 *Contact Pushing of the Particle*

At contact pushing, the forces and equilibrium equations are:

$$
\begin{aligned}
&F_{ta}(y(t)) = -2\pi\gamma R_t + N_{ta} \ , \\
&F_{as}(y(t)) = -4\pi\gamma R_a + N_{as} \ , \\
&-f_{as}(t) - f_{ta}(t)sin\beta + F_{ta}(t)cos\beta = 0 \ , \\
&-f_{ta}(t)cos\beta - F_{ta}sin\beta + F_{as} = 0 \ , \\
&(f_{as}(t) - f_{ta}(t))R_a - f_\theta = 0 \ ,
\end{aligned} \tag{12}
$$

where $y(t)$ is the horizontal sample motion which depends on the motion speed V and resolution Δ, N_{ta} and N_{as} are the tip-particle and particle-substrate repulsive contact forces respectively, and f_θ is the shearing moment resistance between the particle and substrate. During the pushing operations following motion modes with their conditions may exist:

- **Sliding Case:** For the sliding of the particle on the substrate, $f_{as} \geq \mu(F_{as} + 4\pi\gamma R_a)$ condition should be provided. For the tip-particle sliding, $f_{ta} \geq \mu^{'}(F_{ta} + 2\pi\gamma R_t)$ condition exists ($\mu^{'}$ is the maximum static friction coefficient for the tip-particle interface).
- **Sticking Case:** The particle is stuck to the substrate if $f_{as} < \mu(F_{as} + 4\pi\gamma R_a)$, and tip and particle are stuck if $f_{ta} < \mu^{'}(F_{ta} + 2\pi\gamma R_t)$.
- **Rotation Case:** If $f_\theta \geq \mu_\theta A_{as}$, then the particle can realize rolling motion (μ_θ is the rotational shear strength of the particle-substrate contact points, and A_{as} is the contact area between the particle and substrate).

These cases are also analyzed by Saito et al. [8] for picking/releasing particles under SEM. For the precise 2-D positioning of the particles on the substrate by stopping the particle, the tip and particle should stick, particle should slide on the substrate, and particle should not rotate. In other words:

$$
\begin{aligned}
&f_{as}(t) \geq \mu F_{as}(t) \ , \\
&f_{ta}(t) < \mu^{'} F_{ta}(t) \ , \\
&f_\theta(t) < \mu_\theta A_{as}(t) \ .
\end{aligned} \tag{13}
$$

Using the Eq. (12), and $A_{as} = \pi(R_a(F_{as} + 4\pi\gamma R_a)/K)^{2/3}$ by the Hertz contact model, regarding to N_{ta} and f_{ta}, above conditions become as:

$$
\begin{aligned}
&C_1: \ F_{ta} \geq c_1 f_{ta} \ , \\
&C_2: \ F_{ta} > f_{ta}/\mu^{'} \ , \\
&C_3: \ F_{ta}cos\beta - (1 + sin\beta)f_{ta} < \mu_\theta^{'}/R_a(F_{ta}sin\beta + f_{ta}cos\beta + 4\pi\gamma R_a)^{2/3} \ ,
\end{aligned} \tag{14}
$$

where $\mu_\theta^{'} = \pi(R_a/K)^{2/3}\mu_\theta$, $c_1 = (\mu cos\beta + sin\beta)/(cos\beta - \mu sin\beta)$, and C_i represents the condition i. Here, there is a critical value for the C_1 if $\mu = cot\beta$ such that if $\mu < cot\beta$ then C_1 is always

wrong, and if $\mu > cot\beta$, C_1 is always true. For satisfying the above conditions regarding to the μ critical value, F_{ta} and f_{ta} values are plotted where the sliding and rolling without slipping regions are shown as the filled regions (not filled regions all correspond to the rolling with slipping case) in Figure 10 for the values of $R_t = 30\ nm$, $R_a = 0.5\ \mu m$, $\gamma = 0.072\ J/m^2$, $\mu = \mu^{'}$, $\mu_\theta = 30\ N/m$, $K = 23\ GPa$, and $\beta = 26.5^o$. In Figure 10a, $\mu = 2.2 > cot\beta$, and in Figure 10b, $\mu = 0.8 < cot\beta$ where $cot\beta = 2$. Thus, C_1 is always held in Figure 10a, and can be partially held depending on f_{ta} values in Figure 10b. In the figures, depending on the amount of applied load and friction, rolling is also possible.

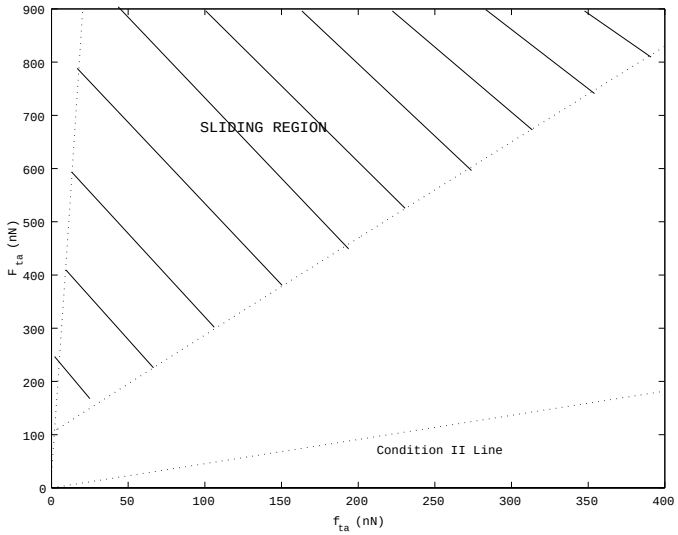

(a)

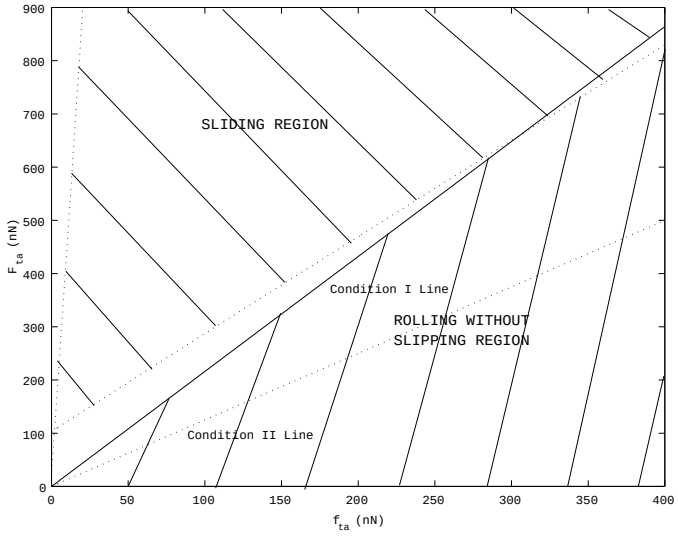

(b)

Figure 10: The particle motion behavior depending on the initial applied load and friction amount: (a) the sliding and rolling regions for $\mu > cot\beta$, and (b) for $\mu < cot\beta$.

During the contact pushing, the cantilever bending force is important for understanding the pushing force and cantilever dynamics. At the equilibrium points, the contact forces deflect the cantilever along the z_c axis as:

$$F_n(t) = (sin\psi + \lambda cos\psi)F_{ta}(t) + (cos\psi - \lambda sin\psi)f_{ta}(t) \ , \tag{15}$$

where $\lambda = 1.5L_y/L_z$ is the structural constant of the cantilever with the cantilever length L_y and tip height L_z respectively, and $\psi = \beta - \alpha$ is the half-angle of the conic tip apex ($\psi = 16.5^o$ in our conic tip). From the deflection data, the shearing point of the particle-substrate interface can be measured. Thus, it is useful to compute the shearing point force values for experimental matching. At the shearing instant $f^*_{as} = \mu F^*_{as}$ ('*' notation shows the values at the shearing point) such that

$$\begin{aligned} &F^*_{ta} = c_1 f^*_{ta} \ , \\ &f^*_{as} = (c_1 cos\beta - sin\beta) f^*_{ta} \ , \\ &\mu^{'} > 1/c_1 \ , \\ &F^*_n = (sin\psi + \lambda cos\psi + (cos\psi - \lambda sin\psi)/c_1) F^*_{ta} \end{aligned} \tag{16}$$

where it is assumed that the tip-particle interface is not sliding, and $\beta \in [0, \pi/2)$. For $\mu = \mu^{'}$, $\mu^{'} > 1/c_1$ condition becomes as $\mu > (1 - sin\beta)/cos\beta$. Thus, ζ^* values are directly proportional to F^*_{ta} and f^*_{as}. Furthermore, there is also a torsion τ_c on the cantilever due to the contact force along the x_c axis where it can not be measured by the present hardware.

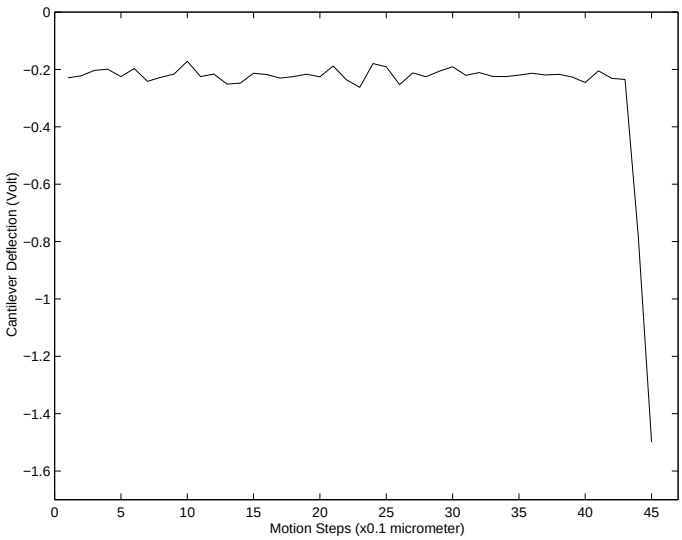

Figure 11: The cantilever deflection during automatic contact detection.

5 Experiments

As the first experiment, the contact point detection is tested. As the initial calibrations, the coordinate transformation parameters are computed as $\alpha_x = \alpha_y = 0.095$, $\phi = -3^o$, $\gamma = -2.5^o$, and the tip center is $(320, 304)$ $pixel$. The cantilever parameters are $R_t = 30\ nm$, $S = 34\ nm/V$, $V_{off} = 3.62\ V$, and $k_c = 8\ N/m$, $L_y = 155\ \mu m$, and $L_z = 4\ \mu m$. The motion speed of the Stage I is around $V = 3.3\ \mu m/sec$ for $\Delta = 0.1\ \mu m$ and $T_s = 30\ msec$. A particle is moved along a line that passes through the tip center, and $\zeta(Volt)$ is observed as in Figure 11. In the figure, $-0.2\ V$ is the no deflection line where around the 43^{th} step of motion the particle contacts and bends until to $-1.5\ V$ which is the ζ_{set} for automatic contact detection. At this point stage stops moving.

As the next experiment, positioning of 2.02 and 1 μm size gold-coated latex particles absorbed on a silicon substrate is demonstrated. Tip material is also silicon. In Figure 12, the automatic pushing of two particles to form a line shape is realized. Typical manipulation time can be computed approximately as $t = (\Delta L/\Delta)T_s$, i.e. $t = 3\ sec$ for $\Delta L = 5\ \mu m$ pushing distance, $T_s = 30\ msec$, and $\Delta = 0.05\mu m$. Next, a 1 μm size particle is pushed 2.4 μm ahead as can be seen in Figure 13 where the deflection force data during the pushing operation is shown in Figure 14. This behavior of the curve is the example of the particle sliding on the surface without rolling case where the initial static friction peak is followed by an almost horizontal sliding line (for the rotation, a sinusoidal deflection, and for a stick-slip motion, a saw-like shape would occur). Moving the substrate along the y-axis, the point **A** is the *contact point*, **B** is the *shearing point* where the particle is detached from the substrate by overcoming the static friction, and starts to slide afterwards, and **C** is the sliding region end point. At point **B**, $F_n^* \approx 461.4\ nN$, and thus $F_{ta}^* = 607.1\ nN$, and $f_{ta}^* = 281\ nN$ are computed by the parameter values of $\alpha = 10^o$, $\psi = 16.5^o$, $\beta = 26.5^o$, $\lambda = 0.0387$, $R_a = 0.5\ \mu m$, $\mu_\theta = 30\ N/m$, $K = 23\ GPa$, and $\mu = \mu^{'} = 0.8$. During this separation phenomenon [19]:

$$f_{as}^* = \kappa A_{as}^* \ , \tag{17}$$

where κ is the shear strength of the contact points. Using the computed F_{ta}^* value, $f_{as}^* = 417.9\ nN$ and $A_{as} = 2.9 \times 10^{-15}\ m^2$ (contact radius of 30.4 nm) are computed where $\kappa = 144 \times 10^6 N/m^2$ in the case of water layer between the particle and substrate. For no rolling motion, $\mu_\theta > \kappa R_a(1 - 1/(c_1 cos\beta - sin\beta))$ should be satisfied where $\mu_\theta > 23.5$ for the given parameter values.

For comparing the theoretical conditions and the experimental results, sliding curve can be investigated. During sliding, $f_{as} = \mu_k F_{as} = (c_2 cos\beta - sin\beta) f_{ta}$ where $\mu_k = 0.7$ is the kinetic friction coefficient, and $c_2 = (\mu_k cos\beta + sin\beta)/(cos\beta - \mu_k sin\beta)$, $F_{ta} = c_2 f_{ta}$, F_n is computed from Eq. (16) by replacing c_1 by c_2, and other tip-particle sticking and no rotation conditions should be satisfied. From Figure 14, for $F_n = 150\ nN$ during sliding, $F_{ta} = 182.7\ nN$, $f_{ta} = 99.2\ nN$, $f_{as} = 119.2\ nN$, and $F_{as} = 170.3\ nN$ are computed. These values satisfy the conditions in Eq. (16) provided that $\mu^{'} > 1/c_2$ and $\mu_\theta > 5.6$. Thus, the sliding behavior is also confirmed by the analysis.

In some cases, if the contact point of the particle and tip is not well centered, i.e. does not pass through the particle center, the particles can be pushed shortly, and then the tip can lose its contact with the particle as shown in Figure 15. This behavior can be due to the particle rotation

along the vertical axis, or sliding along the x_c axis. For avoiding this problem, all calibration parameters are computed with the possible minimum error, and Δ is decreased for reducing positioning errors. Moreover, pushing can break the cantilever tip sometimes due to very large F_{ta}. This possibility is minimized by checking the ζ during pushing such that if it exceeds $-10\ V$, which is also the saturation voltage of the amplifier, then the pushing is stopped, and the design of the particle and substrate should be changed according to the force analysis by changing the environment parameters such as adding lubricants between the particle and substrate, realizing the manipulation in a liquid environment, and etc.

6 Conclusion

In this paper, a fine particle manipulation system using a piezoresistive AFM cantilever as the manipulator and force sensor, and a top-view OM as the vision sensor is proposed. Modeling and control of the AFM cantilever tip and particle interaction has been realized for moving particles with sizes less than 3 μm on a silicon substrate in 2-D. Particle manipulation experiments are realized using a task-based user interface with real-time OM images, and it is shown that the system can be utilized in 2-D micro particle assembling.

Fine particle assembly systems with precise mechanical manipulation capability would enable a powerful tool for future man-made materials and devices. However still there are many challenging problems such as 3-D manipulation, fast, repeatable and reliable autonomous manipulation control, micro/nanophysics-based and compact new gripper design and fabrication, real-time monitoring at the nano scale, and etc. 3-D manipulation is aimed at pick-and-place manipulation, where the gripper design, position control and visual and force sensing are important problems. This work introduces the concept of self-sensing grippers which can be doubled, and utilized as mechanical grippers with visual and force sensing capabilities. For the autonomous control, intelligent strategies integrated with real-time visual and/or force feedback should be developed. Finally, only mechanical manipulation would be limited for functional material and device fabrication, and it should be integrated with other chemical or physical processes such as self-assembly and optical trapping.

Acknowledgements

The authors would like to thank Park Scientific Instruments Co. for providing the piezoresistive cantilevers.

References

[1] H. Miyazaki and T. Sato, "Pick and place shape forming of three-dimensional micro structures from fine particles," in *Proc. of the IEEE Int. Conf. on Robotics and Automation*, pp. 2535–2540, Minneapolis, MN, USA, Apr. 1996.

[2] T. Tanikawa, T. Arai, and T. Masuda, "Development of micro manipulation system with two-finger micro hand," in *Proc. of the IEEE/RSJ Int. Conf. on Intelligent Robots and Systems*, pp. 850–855, Osaka, Japan, 1996.

[3] I. Pappas and A. Codourey, "Visual control of a microrobot operating under a microscope," in *Proc. of the IEEE/RSJ Int. Conf. on Intelligent Robots and Systems*, pp. 993–1000, Osaka, Japan, 1996.

[4] M. Sitti and H. Hashimoto, "Two-dimensional fine particle positioning using a piezoresistive cantilever as a micro/nano-manipulator," in *Proc. of the IEEE Int. Conf. on Robotics and Automation*, pp. 2729–2735, Detroit, USA, May 1999.

[5] F. Arai, D. Ando, and T. Fukuda, "Micro manipulation based on micro physics: Strategy based on attractive force reduction and stress measurement," in *Proc. of the IEEE Int. Conf. on Robotics and Automation*, pp. 236–241, Pittsburgh, USA, 1995.

[6] T. Kasaya, H. Miyazaki, S. Saito, and T. Sato, "Micro object handling under sem by vision-based automatic control," in *Proc. of the IEEE Int. Conf. on Robotics and Automation*, pp. 2189–2196, Detroit, USA, 1999.

[7] Y. Zhou and B. J. Nelson, "Adhesion force modeling and measurement for micromanipulation," in *SPIE Conf. on Microrobotics and Micromanipulation*, pp. 169–180, Boston, USA, Nov. 1998.

[8] S. Saito, H. Miyazaki, and T. Sato, "Pick and place operation of a micro object with high reliability and precision based on micro physics under sem," in *Proc. of the IEEE Int. Conf. on Robotics and Automation*, pp. 2736–2743, Detroit, USA, 1999.

[9] W. Zesch and R. S. Fearing, "Alignment of microparts using force controlled pushing," in *SPIE Conf. on Microrobotics and Micromanipulation*, Boston, USA, Nov. 2-5 1998.

[10] Y. Zhou, B. J. Nelson, and B. Vikramaditya, "Fusing force and vision feedback for micromanipulation," in *Proc. of the IEEE Int. Conf. on Robotics and Automation*, pp. 1220–1225, Leuven, Belgium, 1998.

[11] T. Junno, K. Deppert, L. Montelius, and L. Samuelson, "Controlled manipulation of nanoparticles with an atomic force microscopy," *Appl. Physics Letters*, vol. 66, pp. 3627–3629, June 1995.

[12] M. Sitti and H. Hashimoto, "Force-controlled pushing of nanoparticles using afm," in *Proc. of the IEEE/ASME Int. Conf. on Advanced Intelligent Mechatronics*, pp. 13–20, Atlanta, USA, Sept. 1999.

[13] T. R. Ramachandran, C. Baur, A. Bugacov, and et al., "Direct and controlled manipulation of nanometer-sized particles using the non-contact atomic force microscope," *Nanotechnology*, vol. 9, pp. 237–245, 1998.

[14] M. Sitti and H. Hashimoto, "Tele-nanorobotics using atomic force microscope," in *Proc. of the IEEE/RSJ Int. Conf. on Intelligent Robots and Systems*, pp. 1739–1746, Victoria, Canada, Oct. 1998.

[15] M. Sitti, "Teleoperated 2-d micro/nanomanipulation using atomic force microscope," *Ph.D. Thesis*, Dept. of Electrical Engineering, University of Tokyo, Tokyo, Sept. 1999.

[16] M. Sitti, K. Hirahara, and H. Hashimoto, "2-d micro particle assembly using atomic force microscope," in *Proc. of the IEEE Int. Symp. on Micro Machine and Human Science*, pp. 143–148, Nagoya, Japan, Nov. 1998.

[17] F. J. Giessibl and B. M. Trafas, "Piezoresistive cantilevers utilized for scanning tunneling and scanning force microscope in ultrahigh vacuum," *Rev. Sci. Instrum.*, vol. 65, pp. 1923–1929, June 1994.

[18] J. Israelachvili, *Intermolecular and Surface Forces*. Academic Press London, 2nd ed., 1992.

[19] C. M. Mate, "Force microscopy studies of the molecular origin of friction and lubrication," *IBM J. Res. Develop.*, vol. 39, pp. 617–627, Nov. 1995.

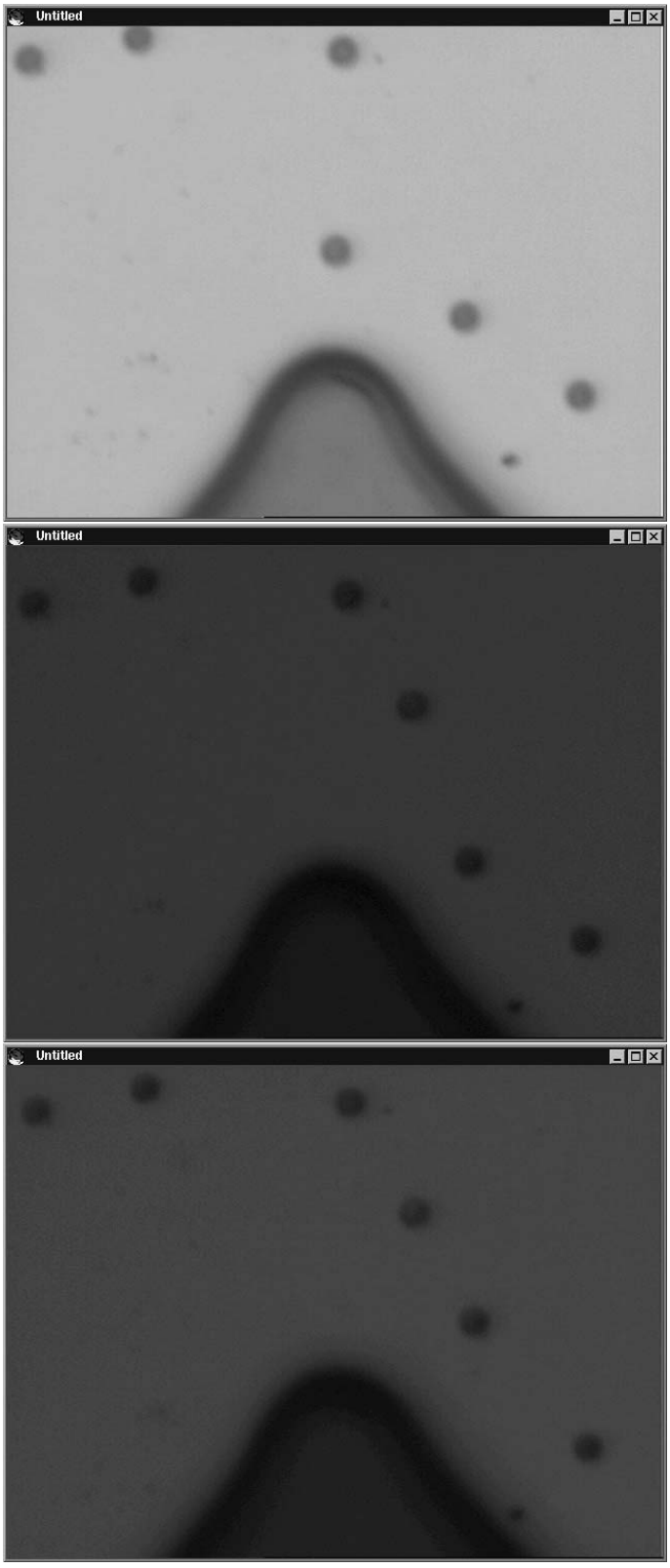

Figure 12: Positioning two particles with 2 μm size: initial positions (uppermost), first pushing (middle), and second pushing (lowermost).

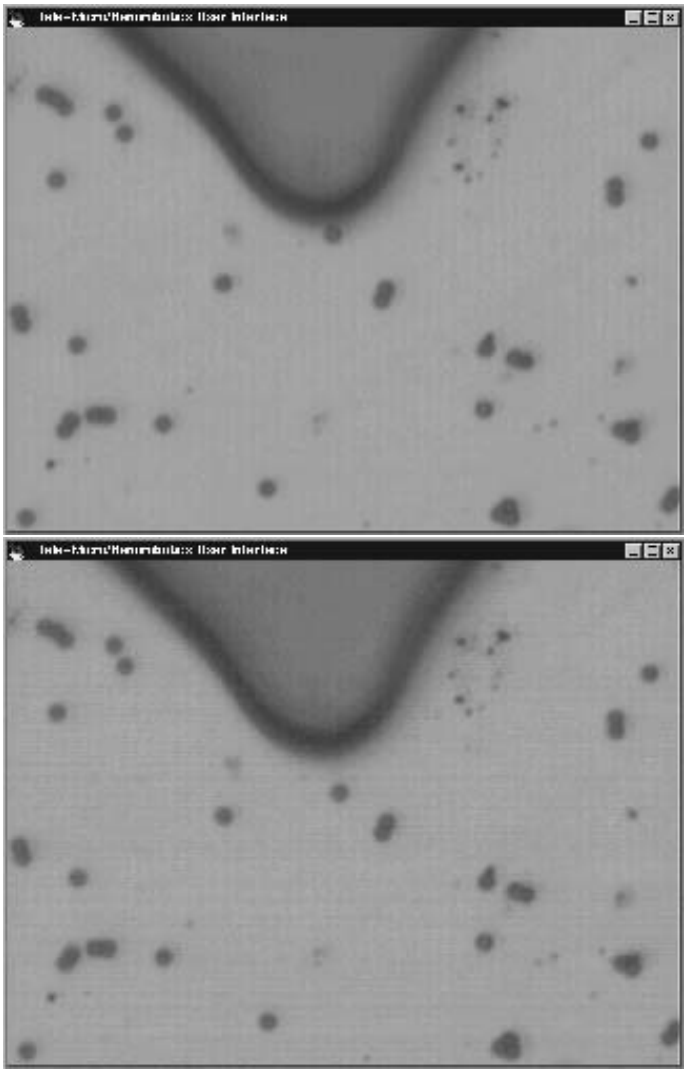

Figure 13: Pushing a 1 μm size particle 2.4 μm distance: initial (upper) and final (lower) configurations.

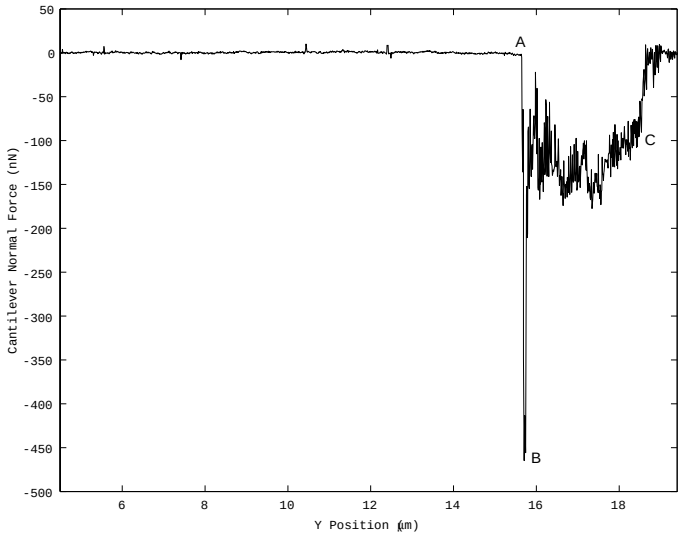

Figure 14: Measured cantilever deflection force during pushing the $1\mu m$ size particle ('-' force values stand for a repulsive/compressive force).

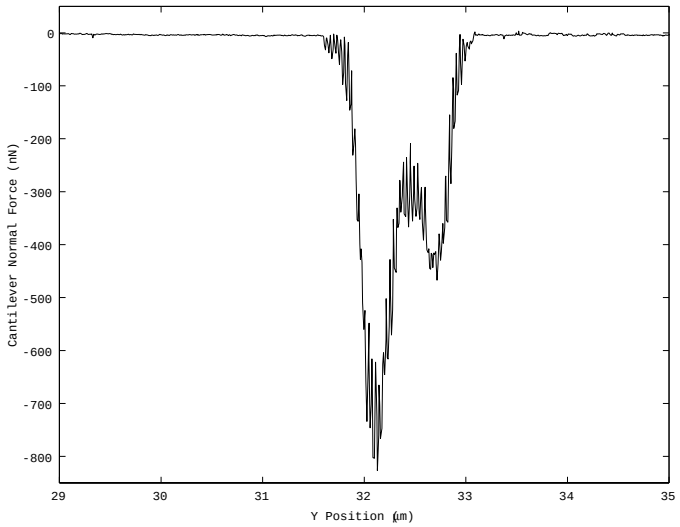

Figure 15: The tip and particle can lose the contact shortly after the initial push due to the pushing direction misalignment.